

Sub-Poissonian statistics of Rydberg-interacting dark-state polaritons

C. S. Hofmann,^{1,*} G. Günter*,¹ H. Schempp*,¹ M. Robert-de-Saint-Vincent,¹
M. Gärttner,^{2,3} J. Evers,² S. Whitlock,^{1,†} and M. Weidemüller^{1,‡}

¹Physikalisches Institut, Universität Heidelberg, Im Neuenheimer Feld 226, 69120 Heidelberg, Germany.

²Max-Planck-Institut für Kernphysik, Saupfercheckweg 1, 69117 Heidelberg, Germany.

³Institut für Theoretische Physik, Universität Heidelberg, Philosophenweg 16, 69120 Heidelberg, Germany
(Dated: December 3, 2012)

Interfacing light and matter at the quantum level is at the heart of modern atomic and optical physics and enables new quantum technologies involving the manipulation of single photons and atoms. A prototypical atom-light interface is electromagnetically induced transparency, in which quantum interference gives rise to hybrid states of photons and atoms called dark-state polaritons. We have observed individual dark-state polaritons as they propagate through an ultracold atomic gas involving Rydberg states. Strong long-range interactions between Rydberg atoms give rise to an effective interaction blockade for dark-state polaritons, which results in large optical nonlinearities and modified polariton number statistics. The observed statistical fluctuations drop well below the quantum noise limit indicating that photon correlations modified by the strong interactions have a significant back-action on the Rydberg atom statistics.

Electromagnetically induced transparency (EIT) is a quantum interference effect in which an otherwise absorbing medium is rendered transparent for a weak probe field by an optical control field [1]. At the few photon level, EIT is characterised by the propagation of coupled excitations of atoms and light called dark-state polaritons (DSPs) [2]. These long-lived quasi-particles simultaneously possess the properties of both the photonic and the atomic degrees of freedom which can be interchanged in a fully coherent and reversible process. As coupled excitations of light and matter, DSPs acquire many new properties from the atomic system. This has been used, for instance, to slow down or even stop light [3–6], to imprint a magnetic moment onto light fields [7], or to realize giant electro-optical effects in atomic vapours [8]. Qualitatively new many-body effects occur when coupling light to *strongly-interacting* atomic systems. Polariton-polariton interactions mediated by the atomic admixture can lead to highly nonlinear [9–11] and nonlocal optical effects [12] as well as the emergence of correlations in both the atomic and the light fields [13, 14]. The ability to produce and coherently control the propagation of quantum fields using interacting dark-state polaritons will open up new applications including few photon nonlinear optics [9, 14, 15], non-classical light sources [10, 13, 16–19], photonic quantum logic gates [19–21], the generation of squeezed states of atomic ensembles [22] and new types of strongly-interacting quantum gases [23–25].

Here we experimentally study both light and matter aspects of strongly interacting DSPs in a dense atomic gas involving highly excited Rydberg states. An important feature of this system is that the Rydberg blockade, in which a single excitation shifts the Rydberg states of nearby atoms out of resonance within a critical distance R_c [26, 27], gives rise to dissipative hard-core interactions and ultimately to correlations between DSPs [14]. In contrast to the usual approach, in which EIT is observed op-

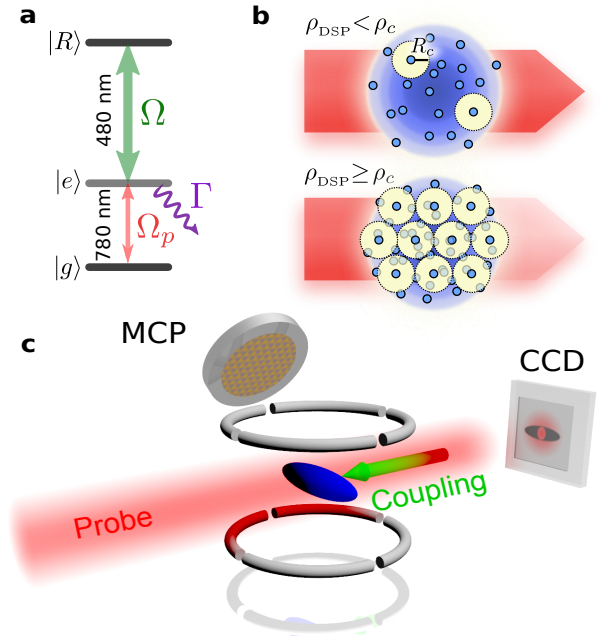


FIG. 1. Experimental setup. **a**, Level scheme used to observe electromagnetically induced transparency in a Rydberg interacting gas. **b**, Cross-section of the atomic cloud (blue) showing the effect of Rydberg blockade on polariton statistics and nonlinear absorption for small and large polariton densities. **c**, Schematic of the experimental setup. The atomic cloud is illuminated by the probe field yielding an absorption image with a local transparency due to the coupling beam. Electrodes (segmented rings) and a micro-channel-plate detector allow for field ionisation and detection of Rydberg atoms.

tically, we explore a new approach which benefits from a high detection sensitivity to Rydberg atoms and directly probes the matter-part of the polariton wavefunction. In this way we extend upon recent work which has shown

the development of nonclassical photon correlations in the transmitted light field [10, 13, 19]. Since the mapping between the properties of the light field and the atomic system is in general non-trivial [10], it is important to study both aspects to obtain a complete picture of EIT in strongly interacting systems. Our experiments cover four orders of magnitude in atomic density which we use to observe the nonlinear optical response and temporal dynamics of polaritons, as well as to investigate the transition to sub-Poissonian polariton statistics when entering the strongly interacting regime. Using a state-of-the-art theoretical approach for the coupled atom-light system we find good agreement with all aspects of the experiment except for the level of sub-Poissonian fluctuations. We observe atomic correlations that are significantly stronger than can be accounted for by assuming the propagation of classical light fields alone. This indicates that the recently observed modification of photon statistics of propagating light fields due to Rydberg interactions [10] can cause a significant back-action on the Rydberg atom statistics.

The basic principle of EIT involves a three-level system (Fig. 1a): two long-lived states $|g\rangle$ and $|R\rangle$ are coupled via a short-lived state $|e\rangle$ which spontaneously decays with rate Γ . Strong laser coupling Ω of the $|e\rangle \rightarrow |R\rangle$ transition creates an Autler-Townes doublet of dressed states, such that the transition amplitudes for the $|g\rangle \rightarrow |e\rangle$ resonance interfere destructively, giving rise to a narrow transparency resonance. This is accompanied by the evolution of the atomic system into a dark-state: a stable superposition of $|g\rangle$ and $|R\rangle$, which is decoupled from the probe field and is thus immune to spontaneous decay. In the weak probe limit, a single probe photon will be partially converted into a collective excitation of the medium to become a dark-state polariton [2],

$$|D_1\rangle = \cos(\theta)|g^{(0)}\rangle - \sin(\theta)|R^{(1)}\rangle, \quad (1)$$

where the collective quantum states involving N atoms and the light field are $|g^{(0)}\rangle = |g_1 \dots g_N\rangle|1\rangle$ and $|R^{(1)}\rangle = 1/\sqrt{N} \sum_{i=1}^N |g_1 \dots R_i \dots g_N\rangle|0\rangle$. The mixing ratio $\tan(\theta) = \sqrt{\rho \sigma c \Gamma} / \Omega$ determines the properties of the polariton depending on the atom density ρ , the resonant scattering cross-section $\sigma = 3\lambda^2/2\pi$, and the speed of light c . The DSP propagates through the atomic medium with negligible loss and reduced group velocity $v_g \approx c/\tan^2(\theta)$.

To understand how interactions between DSPs arise we provide the following simple physical picture (Fig. 1b). For weak probe intensities and for low atomic densities each incident photon is converted into a DSP which propagates freely through the EIT medium before being coherently converted back to the original optical mode. If the light field is subsequently detected on a CCD camera this is observed as transparency of the atomic cloud. For increasing atomic density the group velocity drops ($\theta \rightarrow \pi/2$), effectively compressing the probe field inside the atomic cloud and increasing the density of DSPs ρ_{DSP}

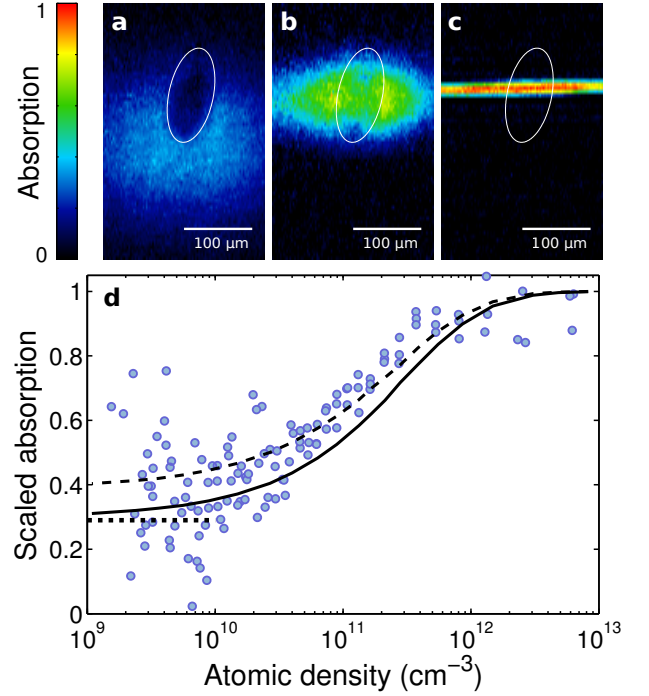


FIG. 2. Nonlinear optical response of the Rydberg EIT medium. Absorption images of the atomic cloud for three expansion times with a probe intensity of $I_p = 5 \mu\text{W}/\text{cm}^2$ and peak densities corresponding to **a**, $5 \times 10^9 \text{ cm}^{-3}$, **b**, $5 \times 10^{10} \text{ cm}^{-3}$ and **c**, $3 \times 10^{12} \text{ cm}^{-3}$. The EIT region illuminated by the coupling laser is indicated by white ellipses. **d** Measured absorption scaled to the two level response as a function of peak atomic density. The dotted horizontal line shows the expected low density EIT absorption due to the finite laser linewidths. The solid and dashed curves are the results of the Monte-Carlo simulations of the coupled atom-light system with $\gamma_{gR}=1.7 \text{ MHz}$ (solid) and $\gamma_{gR}=2.6 \text{ MHz}$ (dashed).

until several begin to occupy the same volume. Since a single polariton includes a large Rydberg state component, it interacts strongly with the Rydberg states of nearby atoms which become shifted out of resonance, breaking the EIT condition for additional excitations and leading to strong inelastic scattering of excess photons from the cloud [13]. This imposes a critical density of DSPs $\rho_c \approx (4\pi R_c^3/3)^{-1}$ corresponding to approximately one per blockade volume, beyond which the density of DSPs saturates (Fig. 1b lower panel).

Our experimental setup is shown schematically in Fig. 1c. We use ^{87}Rb atoms with states $|g\rangle = |5S_{1/2}, F=2\rangle$, $|e\rangle = |5P_{3/2}, F=3\rangle$ with $\Gamma = 6.1 \text{ MHz}$, and the Rydberg state $|R\rangle = |55S_{1/2}\rangle$ which has a lifetime of $\approx 80 \mu\text{s}$. We prepare a cigar shaped cloud of approximately 5×10^4 atoms at a temperature of $5 \mu\text{K}$ in an optical trap. The atomic cloud is uniformly illuminated from the side by a circularly-polarized probe beam with intensity $I_p = 5 \mu\text{W}/\text{cm}^2$ and the transmitted light is imaged onto a CCD camera with an optical resolution

of $\approx 12 \mu\text{m}$ (Rayleigh criterion). The coupling laser is counter aligned to the probe beam and passed through a diffractive optical element to create an approximately uniform intensity profile with $\Omega = 5.1 \text{ MHz}$ over an elliptical region of $\approx 65 \times 130 \mu\text{m}^2$. The frequencies of both lasers are tuned to the atomic resonances. The measured linewidths (including both decay and dephasing terms) for the probe transition and the two-photon transition are $\gamma_{eg} \approx 6.4 \text{ MHz}$ and $\gamma_{gR} \approx 1.7 \text{ MHz}$ respectively, which gives an EIT coupling parameter $\mathcal{C} = \Omega^2/(\gamma_{eg}\gamma_{gR}) = 2.4$ and an EIT resonance width of $w = (1 + \mathcal{C})\gamma_{gR} = 5.8 \text{ MHz}$. The anticipated blockade radius is $R_c = (2C_6/w)^{1/6} \approx 5 \mu\text{m}$ with the van-der-Waals interaction strength $C_6 \approx 50 \text{ GHz } \mu\text{m}^6$. To control the atomic density before pulsing on the probe light we switch off the optical trap and vary the time-of-flight between $20 \mu\text{s}$ and 4.5 ms , varying the peak density (along the line-of-sight) between $\rho \approx 10^{13} - 10^9 \text{ cm}^{-3}$. This is coupled to a change in the cloud length in the probe direction between $\approx 2 \mu\text{m}$ and $100 \mu\text{m}$ and a change in the optical density of the cloud between 3 (resolution limited) and 0.1.

Figure 2 shows absorption images of the atomic cloud for three expansion times corresponding to three different peak atomic densities. For long time-of-flights (corresponding to low densities $\rho \lesssim 10^{10} \text{ cm}^{-3}$) the cloud has expanded considerably, such that the excitation volume is defined primarily by the intensity profile of the coupling laser. Here we observe a high degree of transparency, which can be attributed to the low density of DSPs. By analysing the images we measure the absorption in both the EIT region and the background region corresponding to the two-level optical response (with susceptibility χ_{2L}). At low densities we find the optical response is linear corresponding to a scaled optical susceptibility $\chi_0/\chi_{2L} = 0.3 \pm 0.1$ which is consistent with the expected on-resonant optical susceptibility in the non-interacting EIT regime $\chi_0/\chi_{2L} = 1/(1 + \mathcal{C}) \approx 0.29$. At densities above $\rho \approx 1 \times 10^{10} \text{ cm}^{-3}$ we start to observe a decrease in the transparency due to interactions. Above $\rho \approx 4 \times 10^{11} \text{ cm}^{-3}$ the EIT spot vanishes almost completely.

The full nonlinear optical response as a function of peak atomic density is shown in Fig. 2d. We observe a transition from transparent to fully absorbing by increasing ρ . This characteristic behaviour resembles that obtained by full many-body calculations of the optical susceptibility in a Rydberg blockaded gas [28]. To make a quantitative comparison between theory and experiment we use an optimised version [29] of the rate equation model originally introduced by Ates *et al.* [30]. We assume random atom positions distributed according to the measured Gaussian cloud shape and use Monte-Carlo sampling to solve for the steady state populations in states $|g\rangle$, $|e\rangle$ and $|R\rangle$ for each atom, taking into account the level shifts due to interactions with nearby Rydberg

atoms. Comparing the simulations to the experiment we find that the effect of nonlinear absorption as the probe propagates through the cloud must be accounted for. Therefore, to solve for the steady state populations for any given atom, we first solve for the local probe intensity which is attenuated by all preceding atoms which in turn depends on their steady state populations. The coupled local probe intensity and steady state populations are then determined recursively.

We find good agreement between the measured optical response and the results of the Monte-Carlo simulations using the calculated interaction strength and all other input parameters determined from independent measurements (Fig. 2d-solid curve). The simulations qualitatively reproduce the observed scaling of the nonlinear absorption, however at intermediate and high densities the scaled absorption is underestimated slightly. The discrepancy could be explained by the combination of experimental uncertainties in the measured dephasing rates, additional density-dependent dephasing of the gR -coherence or by decay to nearby Rydberg states which are no longer directly coupled to the light field. In the low density limit the simulations with the measured value of $\gamma_{gR} = 1.7$ (solid line) are consistent with the experimental data. For comparison we show a fit to the data assuming a larger overall dephasing of $\gamma_{gR}=2.6 \text{ MHz}$ (dashed curve).

In our experiments the DSPs are almost entirely matter-like (in eq. (1) $\cos^2(\theta) \approx 10^{-3} - 10^{-7}$). Therefore, measuring the Rydberg population serves as a projective measurement of the number of polaritons inside the cloud. This is possible by field ionizing the Rydberg states and subsequently detecting the individual ions on a microchannel plate (MCP) detector which provides high time resolution and near single particle sensitivity (Fig. 3a). We apply an electric field just above ionization threshold to field ionize and guide the resultant ions to maximize the spread in arrival times. In a typical experiment we detect ≈ 10 ions. The probability for two ions to arrive simultaneously such that they are miscounted as a single event is less than 1%.

Figure 3b shows the measured time evolution of the number of detected ions during a $2.2 \mu\text{s}$ probe pulse in the non-interacting regime. At short times we observe a rapid increase of the detected ions reflecting the entry of DSPs into the atomic cloud. The observed rise time of $\approx 100 \text{ ns}$ is compatible with the spectral width of the EIT-resonance. After this time the number of detected ions approaches a steady state value of around $\langle N_{\text{ions}} \rangle \approx 10$, which, accounting for our ion detection efficiency ($\eta \approx 0.4$) corresponds to ≈ 25 polaritons inside the cloud. After the pulse the Rydberg state population decreases rapidly, which is expected as the polaritons leave the atomic cloud and are coherently mapped back onto the light field. By analysing the images we confirm that the cloud remains mostly transparent until the elec-

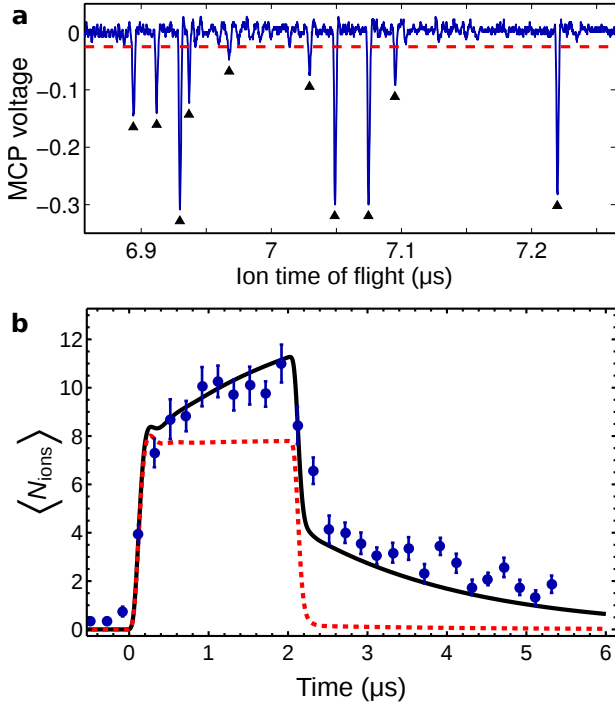


FIG. 3. **Polariton dynamics observed during a $2\ \mu\text{s}$ probe pulse measured via the Rydberg state population.** **a**, Typical ion signal showing the detection of individual ions (marked by triangles). The dashed horizontal line indicates the threshold voltage of $-0.02\ \text{V}$ below which we count voltage spikes as ion detection events. **b**, Measured polariton evolution with each data point computed from the average of 20 runs of the experiment. The vertical error bars represent the statistical error of the mean. The solid line is a fit to the data using the numerical solution to the optical Bloch equations, including a coupling to both Rydberg Zeeman sublevels $m_j = \pm 1/2$ which accounts for the slow evolution and residual Rydberg population after $2\ \mu\text{s}$. The dashed red line shows the population in the resonantly coupled Zeeman state alone.

tric field is switched on. Over the full pulse duration we estimate a total of ~ 1500 polaritons pass through the atomic cloud. After the pulse we observe a residual population of about 30% of the peak number of ions and a slower time evolution. The dashed line in Fig. 3b shows the expected evolution found by solving the three-level optical Bloch equations. The additional slow rise during the pulse and the longer tail observed in the experiment can be attributed to laser coupling to additional Zeeman sublevels assuming polarization dependent coupling strengths (Fig. 3b-solid line).

Now to investigate the appearance of correlations in the strongly interacting regime, we map out the distribution of DSPs inside the cloud as a function of atomic density. After $2\ \mu\text{s}$ of probe laser illumination we turn on the ionization field and count the number of detected ions. This is repeated between 150-300 times for each time-of-flight corresponding to different peak densities of the cloud. From these data we construct histograms of

the ion number distribution (Fig. 4a) which is used to extract the mean and variance of the number of polaritons.

In Fig. 4b we show the measured mean ion number $\langle N_{\text{ions}} \rangle$ which is proportional to the number of DSPs inside the cloud. The low-density behaviour is determined by the changing number of atoms in the excitation volume as a function of time-of-flight (dashed-line). For $\rho > 10^{11}\ \text{cm}^{-3}$ we observe a rapid decrease of $\langle N_{\text{ions}} \rangle$ due to probe laser attenuation and polariton-polariton interactions. The solid-line is the results of the Monte-Carlo simulation using the same parameters as for Fig. 2. To obtain the best agreement we adjust only two parameters in the simulation: the detection efficiency η and the effective area of the coupling laser ellipse. Optimal agreement is found for an elliptical coupling region with minor and major axes of $65\ \mu\text{m}$ and $130\ \mu\text{m}$ respectively, and $\eta = 0.4$ which is consistent with our experimental geometry.

Simultaneous to the onset of the polariton blockade we also observe a significant narrowing of the statistical distribution of the detected ions (Fig. 4a). We quantify this using the Mandel Q parameter

$$Q = \frac{\langle N_{\text{ions}}^2 \rangle - \langle N_{\text{ions}} \rangle^2}{\langle N_{\text{ions}} \rangle} - 1, \quad (2)$$

which compares the width of an observed distribution to a Poisson distribution with the same mean. For a Poissonian process $Q = 0$, whereas a sub-Poissonian process yields $Q < 0$ reflecting the emergence of spatial and temporal correlations [31–33].

Figure 4c shows the measured Mandel Q parameter as a function of the peak density of the atomic cloud. In the low-density limit, polariton-polariton interactions can be neglected and the measured ion number distributions are close to Poissonian with $Q \approx 0$ which is expected for a coherent input light field. Increasing the density we observe a clear transition to sub-Poissonian statistics with Q reaching a minimum value of -0.32 with a statistical uncertainty of 0.04 calculated in the range $2 \times 10^{11}\ \text{cm}^{-3} < \rho < 2 \times 10^{12}\ \text{cm}^{-3}$. Including the effect of imperfect ion detection indicates that the true distribution of DSPs is much narrower corresponding to strong spatial and temporal correlations (since $Q_{\text{DSP}} = Q/\eta$).

Despite the good agreement of the Monte-Carlo model with both the optical response data (Fig. 2d) and the mean number of polaritons (Fig. 4b), it clearly fails to describe the experimentally measured Q parameters which are much lower than predicted (Fig. 4c). We attribute this to the neglected effect of photon correlations (the Monte-Carlo algorithm assumes a classical field at each step characterised by a Rabi frequency Ω_p) which can build up as a consequence of dissipative polariton-polariton interactions [10].

A complete and rigorous many-body treatment of this problem, including the effects of the quantized electro-

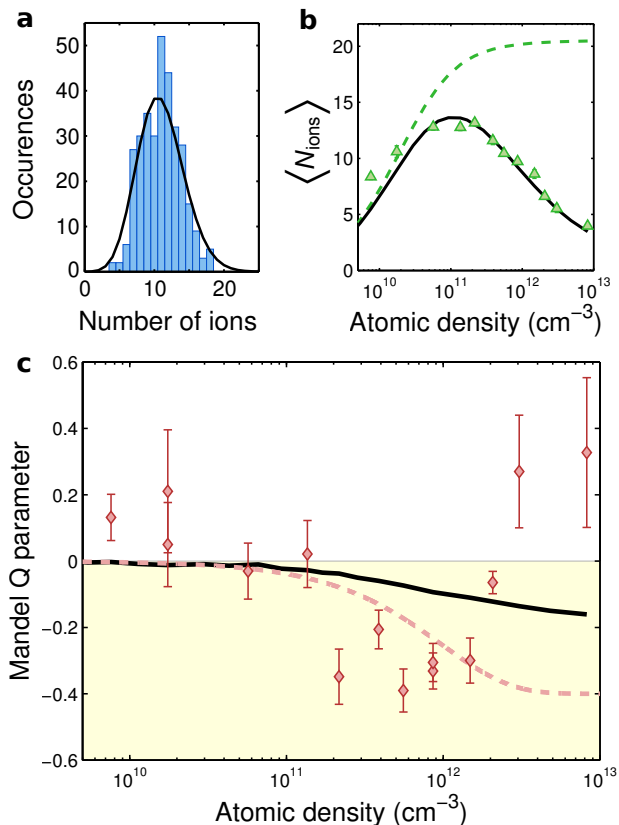


FIG. 4. **Statistical distribution of the detected ions during a 2 μ s probe pulse showing the transition to sub-Poissonian statistics.** **a**, Typical ion number histogram for $\rho = 5 \times 10^{11} \text{ cm}^{-3}$ with $Q = -0.3$ compared to a Poisson distribution with the same mean (solid line). **b**, Measured mean number of ions as a function of atomic density which decreases above $\rho = 10^{11} \text{ cm}^{-3}$ due to blockade. The solid line is the result of the Monte-Carlo calculations with $\eta = 0.4$ and the dashed line shows the Rydberg number neglecting interactions and probe absorption, which is proportional to the total number of atoms in the excitation volume. **c**, In the high density regime the Mandel Q parameter falls to sub-Poissonian values. The solid line is the result of Monte-Carlo calculations using the same parameters as in Fig. 2d and Fig. 4b. The dashed curve is derived from the hard sphere model assuming an initial Poissonian photon number distribution with $\rho_{crit} = 1 \times 10^{12} \text{ cm}^{-3}$. The statistical errors are estimated by dividing the data for each density into 3 subsets of 50 experimental runs each and then calculating the standard error of the mean Q parameter.

magnetic field is still lacking. However, we can make a simple estimate for the possible effects of photon correlations by assuming a hard-sphere model for polariton interactions. We discretize the excitation volume into elements corresponding to the size of a blockade sphere and assume an initial Poisson distribution for the number of photons per element with a mean of $\langle N_{ph} \rangle \approx \frac{\Omega_p^2}{\Omega_c^2} \rho / \rho_c$ [13]. For $N_{ph} \geq 1$ we assume that one DSP is created with unity probability and the excess photons couple to bright

states which do not include a Rydberg state component. Therefore the corresponding DSP statistics range from Poissonian-character for $\langle N_{ph} \rangle \ll 1$ (limited by the classical fluctuations of the laser field) to strongly sub-Poissonian for $\langle N_{ph} \rangle \gg 1$ above the critical density at which the DSP density saturates. The atomic density at which correlations become important is when $\langle N_{ph} \rangle = 1$, which for our experimental parameters corresponds to $\rho_{crit} \approx 1 \times 10^{12} \text{ cm}^{-3}$. According to this simple model we find $Q \approx \eta \exp(-\rho/\rho_{crit}) - \eta$, which is in closer agreement with the data, confirming that the development of photon number correlations within the cloud plays an important role on the DSP statistics (Fig. 4c).

For the largest densities we find that the measured Q values increase again to super-Poissonian values. We have not yet identified the cause of this increase, but we note that it co-incides with the point when the cloud becomes quasi-1D with respect to the Rydberg excitation which might modify the effects of interactions on the propagating light field. Alternatively it could be due to the production of a small number of prompt ions (below our detection sensitivity) [34] which can dramatically affect the polariton statistics. Spurious ions could also be present in recent experiments studying the effects of Rydberg blockade on photon statistics [10, 18, 19] but to our knowledge their effects have not been investigated so far.

Our experiments provide a direct observation of strongly-interacting DSPs realized using EIT in an ultracold Rydberg gas. Strong polariton-polariton interactions are observed through the density dependent optical response and the polariton counting statistics, which become significantly sub-Poissonian at high densities, reflecting the emergence of spatial and temporal correlations between polaritons. The method presented here in principle allows for studying the full polariton counting statistics, thereby also giving access to higher order correlations [31]. Two-photon correlations have recently been observed in the second order intensity correlation function of light $g^{(2)}(\tau)$ retrieved from small Rydberg ensembles [18, 19], and via light propagation through dense atomic clouds [10]. We point out however that in general there is no direct mapping between the correlations on the light field and the atomic correlations. For instance, in a dense but optically thin medium, excess photons may not be efficiently scattered out of the forward direction thereby washing out the $g^{(2)}$ contrast, despite the presence of strong atomic correlations. Alternatively, outside of the blocked regime, spin-wave dephasing due to atomic interactions can alter the statistics of the emitted light [18, 35, 36], even though the atomic correlations could remain nearly classical. A complete description of EIT in strongly-interacting media remains a theoretically challenging problem [10], therefore it is necessary to study both aspects and to provide more stringent tests to theoretical models. Ultimately this would open an av-

enue to on-demand sources of single photons and other nonclassical states of light.

Our experiments can be interpreted as Rydberg dressing of photons, in which photon-photon interactions are mediated by the Rydberg state admixture. By detuning from the intermediate state, the dissipative character of the polariton-polariton interactions could be suppressed while maintaining the huge nonlinearities which would give rise to elastic scattering [14]. As the nonlinearity can be controlled via the choice of the Rydberg state, repulsive, attractive and long-range interactions become possible. This could pave the way to create and study new types of quantum gases such as dipolar Bose-Einstein condensates of dark-state polaritons [24, 25].

METHODS

Coupled atom-light simulations. To model the experiments we use an optimised rate equation model [29]. We simulate the full number of atoms within the coupling volume ($N \approx 5000 - 25000$) assuming random positions distributed according to the measured Gaussian cloud shape. Monte-Carlo sampling is used to solve for the steady state populations for each atom, taking into account the level shifts due to interactions with nearby Rydberg atoms. The probability for an atom to change its state is determined by a stochastic process. In each step an atom is picked randomly and the steady state populations are calculated, taking into account level shifts due to the interaction with nearby Rydberg atoms. To include the effects of probe laser attenuation we first solve for the local Rabi frequency $\Omega_p^{(i)}$ which is attenuated by all other atoms $j < i$ in a cylindrical volume with cross-section A . The degree of attenuation is given by $\Omega_p^{(j+1)} = \Omega_p^{(j)} \exp(-\chi^{(j)})$ where $\chi^{(j)}$ is proportional to the $|e\rangle$ state population for atom j . We recursively determine the local $\Omega_p^{(j)}$ starting with $j = 1$ which sees the total incident probe Rabi frequency $\Omega_p^{(1)}$. We then solve for the steady state populations iteratively until $j = i$. The outcome of this procedure does not depend on the exact choice of A (typically $3 - 10 \mu\text{m}^2$) as long as A is small compared to the size of the atomic cloud.

Counting polaritons. The number of polaritons inside the cloud is measured by field ionizing the Rydberg states and guiding the ions to an MCP detector. The field is switched above the field ionization threshold within 300 ns and the resultant ion trace is recorded on a fast oscilloscope. Each ion creates a voltage spike with a width of ~ 1.5 ns with arrival time distributed over ~ 600 ns. N_{ions} is found by fitting each trace with the MCP transfer function using sparse spikes deconvolution and counting

extrema for pulses with amplitudes less than the threshold voltage of -0.02 V. From the pulse-height-distribution we infer a counting efficiency of 0.9, which combined with the MCP detection efficiency, angular responsivity and guiding efficiency gives an estimated overall efficiency which is in good agreement with the best fit to the data of $\eta \approx 0.4$. For the low numbers of ions produced in our experiment detector saturation can be safely neglected.

* These authors contributed equally to this work

† whitlock@physi.uni-heidelberg.de

‡ weidemueller@uni-heidelberg.de

- [1] Fleischhauer, M., Imamoglu, A., and Marangos, J. P. Electromagnetically induced transparency: Optics in coherent media. *Rev. Mod. Phys.* **77**, 633–673 (2005).
- [2] Fleischhauer, M. and Lukin, M. D. Dark-state polaritons in electromagnetically induced transparency. *Phys. Rev. Lett.* **84**, 5094–5097 (2000).
- [3] Hau, L. V., Harris, S. E., Dutton, Z., and Behroozi, C. H. Light speed reduction to 17 metres per second in an ultracold atomic gas. *Nature* **397**, 594–598 (1999).
- [4] Liu, C., Dutton, Z., Behroozi, C. H., and Hau, L. V. Observation of coherent optical information storage in an atomic medium using halted light pulses. *Nature* **409**, 490–493 (2001).
- [5] Phillips, D. F., Fleischhauer, A., Mair, A., Walsworth, R. L., and Lukin, M. D. Storage of light in atomic vapor. *Phys. Rev. Lett.* **86**, 783–786 (2001).
- [6] Bajcsy, M., Zibrov, A. S., and Lukin, M. D. Stationary pulses of light in an atomic medium. *Nature* **426**, 638–641 (2003).
- [7] Karpa, L. and Weitz, M. A Stern–Gerlach experiment for slow light. *Nature Physics* **2**, 332–335 (2006).
- [8] Mohapatra, A., Bason, M., Butscher, B., Weatherill, K., and Adams, C. A giant electro-optic effect using polarizable dark states. *Nature Physics* **4**, 890–894 (2008).
- [9] Pritchard, J. D., Maxwell, D., Gauguier, A., Weatherill, K. J., Jones, M. P. A., and Adams, C. S. Cooperative atom-light interaction in a blockaded Rydberg ensemble. *Phys. Rev. Lett.* **105**, 193603 (2010).
- [10] Peyronel, T., Firstenberg, O., Liang, Q., Hofferberth, S., Gorshkov, A., Pohl, T., Lukin, M., and Vuletić, V. Quantum nonlinear optics with single photons enabled by strongly interacting atoms. *Nature* (2012).
- [11] Parigi, V., Bimbard, E., Stanojevic, J., Hilliard, A. J., Nogrette, F., Tualle-Brouiri, R., Ourjoumtsev, A., and Grangier, P. Observation and measurement of “giant” dispersive optical non-linearities in an ensemble of cold Rydberg atoms. *arXiv:1209.1948* (2012).
- [12] Sevinçli, S., Henkel, N., Ates, C., and Pohl, T. Nonlocal nonlinear optics in cold Rydberg gases. *Phys. Rev. Lett.* **107**(15), 153001 (2011).
- [13] Petrosyan, D., Otterbach, J., and Fleischhauer, M. Electromagnetically induced transparency with Rydberg atoms. *Phys. Rev. Lett.* **107**, 213601 (2011).
- [14] Gorshkov, A. V., Otterbach, J., Fleischhauer, M., Pohl, T., and Lukin, M. D. Photon-photon interactions via Rydberg blockade. *Phys. Rev. Lett.* **107**, 133602 (2011).
- [15] Shahmoon, E., Kurizki, G., Fleischhauer, M., and Pet-

- rosyan, D. Strongly interacting photons in hollow-core waveguides. *Phys. Rev. A* **83**, 033806 (2011).
- [16] Honer, J., Löw, R., Weimer, H., Pfau, T., and Büchler, H. P. Artificial atoms can do more than atoms: Deterministic single photon subtraction from arbitrary light fields. *Phys. Rev. Lett.* **107**, 093601 (2011).
- [17] Pritchard, J. D., Weatherill, K. J., and Adams, C. S. Non-linear optics using cold Rydberg atoms. *arXiv:1205.4890* (2012).
- [18] Dudin, Y. O. and Kuzmich, A. Strongly interacting Rydberg excitations of a cold atomic gas. *Science* **336**, 887–889 (2012).
- [19] Maxwell, D., Szwer, D., Barato, D., Busche, H., Pritchard, J., Gauguier, A., Weatherill, K., Jones, M., and Adams, C. Quantum state control of stored optical photons. *arXiv:1207.6007* (2012).
- [20] Friedler, I., Petrosyan, D., Fleischhauer, M., and Kurizki, G. Long-range interactions and entanglement of slow single-photon pulses. *Phys. Rev. A* **72**, 043803 (2005).
- [21] Petrosyan, D. and Fleischhauer, M. Quantum information processing with single photons and atomic ensembles in microwave coplanar waveguide resonators. *Phys. Rev. Lett.* **100**, 170501 (2008).
- [22] Opatrny, T. and Mølmer, K. Spin squeezing and Schrödinger-cat-state generation in atomic samples with Rydberg blockade. *Phys. Rev. A* **86**, 023845 (2012).
- [23] Chang, D. E., Gritsev, V., Morigi, G., Vuletić, V., Lukin, M. D., and Demler, E. A. Crystallization of strongly interacting photons in a nonlinear optical fibre. *Nature Physics* **4**, 884 (2008).
- [24] Fleischhauer, M., Otterbach, J., and Unanyan, R. G. Bose-Einstein condensation of stationary-light polaritons. *Phys. Rev. Lett.* **101**, 163601 (2008).
- [25] Nikoghosyan, G., Zimmer, F. E., and Plenio, M. B. Dipolar Bose-Einstein condensate of dark-state polaritons. *Phys. Rev. A* **86**, 023854 (2012).
- [26] Lukin, M. D., Fleischhauer, M., Cote, R., Duan, L. M., Jaksch, D., Cirac, J. I., and Zoller, P. Dipole blockade and quantum information processing in mesoscopic atomic ensembles. *Phys. Rev. Lett.* **87**, 037901 (2001).
- [27] Comparat, D. and Pillet, P. Dipole blockade in a cold Rydberg atomic sample. *J. Opt. Soc. Am. B* **27**, A208–A232 (2010).
- [28] Ates, C., Sevinçli, S., and Pohl, T. Electromagnetically induced transparency in strongly interacting Rydberg gases. *Phys. Rev. A* **83**, 041802 (2011).
- [29] Heeg, K. P., Gärttner, M., and Evers, J. A hybrid model for Rydberg gases including exact two-body correlations. *arXiv:1202.2779* (2012).
- [30] Ates, C., Pohl, T., Pattard, T., and Rost, J. M. Many-body theory of excitation dynamics in an ultracold Rydberg gas. *Phys. Rev. A* **76**, 013413 (2007).
- [31] Ates, C., Pohl, T., Pattard, T., and Rost, J. Strong interaction effects on the atom counting statistics of ultracold Rydberg gases. *J. Phys. B: At. Mol. Opt. Phys.* **39**, L233 (2006).
- [32] Reinhard, A., Younge, K. C., and Raithel, G. Effect of Förster resonances on the excitation statistics of many-body Rydberg systems. *Phys. Rev. A* **78**, 060702 (2008).
- [33] Viteau, M., Huillery, P., Bason, M. G., Malossi, N., Ciampini, D., Morsch, O., Arimondo, E., Comparat, D., and Pillet, P. Cooperative excitation and many-body interactions in a cold Rydberg gas. *Phys. Rev. Lett.* **109**, 053002 (2012).
- [34] Robert-de-Saint-Vincent, M., Hofmann, C. S., Schempp, H., Günter, G., Whitlock, S., and Weidemüller, M. Spontaneous avalanche ionization of a strongly blocked Rydberg gas. *arXiv:1209.4728* (2012).
- [35] Dudin, Y. O., Bariani, F., and Kuzmich, A. Emergence of spatial spin-wave correlations in a cold atomic gas. *Phys. Rev. Lett.* **109**, 133602 (2012).
- [36] Bariani, F., Goldbart, P. M., and Kennedy, T. A. B. Dephasing dynamics of Rydberg atom spin waves. *Phys. Rev. A* **86**, 041802 (2012).

Acknowledgements We acknowledge N. Müller, A. Faber and H. Busche for contributions to the experimental apparatus, K. Heeg for work on the theoretical model, T. Pohl for valuable discussions and J.-W. Pan and S. Jochim for reading the manuscript. This work is supported in part by the Heidelberg Center for Quantum Dynamics and supported by the Deutsche Forschungsgemeinschaft under WE2661/10.2. M.R.D.S.V. acknowledges support from the EU Marie-Curie program (Grant No. FP7-PEOPLE-2011-IEF-300870).

Author contributions C.S.H, G.G and H.S constructed the experimental apparatus and together with M.R.D.S.V and S.W. took the experimental data. M.G and J.E developed the theoretical model. All authors discussed and analysed the data and jointly wrote the manuscript.